

ACTIVE GALACTIC NUCLEI WITH DOUBLE-PEAKED BALMER LINES: I. BLACK HOLE MASSES AND THE EDDINGTON RATIOS

WEI-HAO BIAN^{1,2}, YAN-MEI CHEN¹, QIU-SHENG GU³, AND JIAN-MIN WANG¹

Submitted to ApJ

ABSTRACT

Using the stellar population synthesis, we model the stellar contribution for a sample of 110 double-peaked broad-lines AGNs from the Sloan Digital Sky Survey (SDSS). The stellar velocity dispersions (σ_*) are obtained for 52 double-peaked AGNs with obvious stellar absorption features, ranging from 106 to 284 km s⁻¹. We also use multi-component profiles to fit [O III] $\lambda\lambda 4959, 5007$ and H β emission lines. Using the well-established $M_{\text{bh}} - \sigma_*$ relation, the black hole masses are calculated to range from 1.0×10^7 to $5.5 \times 10^8 M_\odot$, and the Eddington ratio from about 0.01 to about 1. Comparing with the known $R_{\text{BLR}} - L$ relation, we can get the factor f , which indicates BLRs' geometry, inclination and kinematics. We find that f far deviates from 0.75, suggesting the non-virial dynamics of broad line regions. The peak separation is mildly correlated with the Eddington ratio and SMBH mass with almost the same correlation coefficients. It implies that it is difficult to detect obvious double-peak AGNs with higher Eddington ratios. Using the monochromatic luminosity at 5100Å to trace the bolometric luminosity, we find that the external illumination of the accretion disk is needed to produce the observed strength of H α emission line.

Subject headings: galaxies:active — galaxies: nuclei — black hole physics — accretion, accretion disks

1. INTRODUCTION

Double-peaked broad Balmer emission profiles have been detected in about 200 active galactic nuclei (AGNs) (Eracleous & Halpern 1994, 2003; Strateva et al. 2003, 2006). A systematic survey of 110 sources (mostly broad-line radio loud AGNs at $z < 0.4$) by Eracleous & Halpern (1994, 2003) suggested that about 20% sources show double-peaked broad Balmer lines. They found some characteristics of double-peaked AGNs: large full width at half maximum (FWHM) of H α line, ranging from about 4000 km s⁻¹ up to 40000 km s⁻¹ (e.g. Wang et al. 2005); about 50% starlight contribution in optical continuum around H α ; large equivalent widths of low-ionization forbidden lines; large [O I]/[O III] ratios. Strateva et al. (2003) found about 3% of the $z < 0.332$ AGNs in the Sloan Digital Sky Survey (SDSS) are double-peaked AGNs, the fraction is smaller than that in radio-loud AGNs sample. Double-peaked lines have also been detected in some low-ionization nuclear emission line regions (LINERs), e.g. NGC1097, M81, NGC4450, NGC4203, NGC4579 (Storchi-Bergmann et al. 1993; Bower et al. 1996; Shields et al. 2000; Ho et al. 2000; Barth et al. 2001). It remains a matter as debate of the origin of the double-peaked profiles.

There are mainly three models to interpret the origin of the double-peaked profiles: the accretion disk (Chen & Halpern 1989; Eracleous & Halpern 1994, 2003; Gezari et al. 2007); the biconical outflow (Zheng et al. 1991; Abajas et al. 2006), and an anisotropic illuminated BLRs (Goad & Wanders 1996). More recently, observational

test and physical consideration preferentially suggested that double-peaked profiles originate from the accretion disk within a radius from a few hundreds R_g to about thousands R_g ($R_g = GM_{\text{bh}}/c^2$, M_{bh} is the SMBH mass) (Eracleous & Halpern 1994, 2003; Eracleous et al. 1997; Strateva et al. 2003, 2006; Gezari, et al. 2007). In order to interpret the sparsity of double-peaked AGNs, the origin of the single-peaked lines from accretion disk have been discussed (Eracleous & Halpern 2003 and the references therein): larger out radius of the line-emitting accretion disk; face-on accretion disk; and the accretion disk wind. Very few of the double-peaked high-ionization line profiles (e.g. CIV) is due to that these high ionization lines are thought to arise in a wind, not in the disk.

The masses of central supermassive black holes (SMBHs) can provide an important tool to understand the physics of double-peaked AGNs if we reliably estimate them (e.g. Lewis & Eracleous 2006; Lewis 2006). During the last decade, there is a striking progress on the study of central supermassive black holes. The stellar and/or gaseous dynamics is used to derive the SMBHs masses in nearby inactive galaxies. However, for AGNs, this method is very difficult because nuclei outshine their hosts. Fortunately, we can use the broad emission lines from BLRs (e.g. H β , H α , Mg II, CIV) to estimate SMBH masses in AGNs by the reverberation mapping method and the empirical size-luminosity relation (Kaspi et al. 2000, 2005; Vestergaard 2002; McLure & Jarvis 2002; Wu et al. 2004; Greene & Ho 2006a). There is a scaling factor with larger uncertainty, which is due to the unknown geometry and dynamics of broad line regions, BLRs (e.g. Krolik 2001; Collin et al. 2006). Nearby galaxies and AGNs seem to follow the same tight $M_{\text{bh}} - \sigma_*$ relation, where σ_* is the bulge velocity dispersion at eighth of the effective radius of the galaxy (Nelson et al. 2001; Tremaine et al. 2002; Greene & Ho 2006a, 2006b), although it remains controversial for narrow-line Seyfert

¹ Key Laboratory for Particle Astrophysics, Institute of High Energy Physics, Chinese Academy of Sciences, Beijing 100039, China

² Department of Physics and Institute of Theoretical Physics, Nanjing Normal University, Nanjing 210097, China; wh-bian@njnu.edu.cn

³ Department of Astronomy, Nanjing University, Nanjing 210093, China

1 galaxies (NLS1s) (Mathur et al. 2001; Bian & Zhao 2004; Grupe & Mathur 2004; Watson et al. 2007). Lewis & Eracleous (2006) derived the black hole masses from σ_* through fitting absorption lines of the Ca II triplet ($\lambda\lambda 8498, 8542, 8662$) for 5 double-peaked AGNs. Therefore the determination of the black hole mass from independent method of reverberation mapping is an useful probe to explore mysteries of the double peaked AGNs.

Significant stellar contribution in double-peaked AGNs makes the measurement of σ_* possible and reliable. Here we present our results on the σ_* measurements for the sample of 110 double-peaked AGNs from the Sloan Digital Sky Survey (SDSS) (Strateva et al. 2003). In section 2, we introduce our working sample selected from Strateva et al. (2003). Section 3 is data analysis. We present the calculations of the SMBH mass and the Eddington ratio, and discuss their errors in Section 4. Section 5 is contributed to the discuss of the BLRs in double-peaked AGNs. Section 6 is the relation between the peak separation and Mass/Eddington ratio. Section 7 is the Energy budget for double-peaked AGNs. Our conclusion is given in Section 8. The last section is our conclusion. All of the cosmological calculations in this paper assume $H_0 = 71 \text{ km s}^{-1} \text{ Mpc}^{-1}$, $\Omega_M = 0.27$, and $\Omega_\Lambda = 0.73$.

2. SAMPLE

Strateva et al. (2003) presented a sample of double-peaked AGNs ($z < 0.332$) selected from SDSS. They used two steps to select candidates: (1) they selected the unusual ones from the symmetric lines using the spectral principal component analysis (PCA) (Hao et al. 2003); and (2) they fitted the H α region with a combination of several Gaussians, and only selected AGNs better fitted by two Gaussians. From the profiles of the broad components, several fitting parameters including the positions of the red and blue peaks ($\lambda_{\text{red}}, \lambda_{\text{blue}}$), the corresponding peak heights ($H_{\text{red}}, H_{\text{blue}}$), FWHMs were given in their Table 3. They investigated the multi-wavelength properties of these double-peaked AGNs and suggested that Eddington ratios could be large in these SDSS double-peaked AGNs (Strateva et al. 2006).

SDSS spectra cover the wavelength range of 3800-9200 Å with a spectral resolution of $1800 < R < 2100$. The fiber diameter in the SDSS spectroscopic survey is 3" on the sky. At the mean redshift of 0.24 in the sample of Strateva et al. (2003), the projected fiber aperture diameter is 13.2 kpc, typically containing about 80% of the total host galaxy light (Kauffmann & Heckman 2005). The stellar absorption features in these SDSS spectra provide us the possibility to measure the stellar velocity dispersion. We did not apply aperture corrections to the stellar velocity dispersions because this effect can be omitted for $z < 0.3$ (Bernardi et al. 2003; Bian et al. 2006).

3. DATA ANALYSIS

There are a number of objective and accurate methods to measure σ_* , including two main different techniques, the "Fourier-fitting" method (Sargent et al. 1977; Tonry & Davis 1979), and the "direct-fitting" method (Rix & White 1992; Greene & Ho 2006b and reference therein). With the development of computing, the "direct-fitting" method become much more popular. For SDSS spectra

with significant stellar absorption features (such as Ca H+K $\lambda\lambda 3969, 3934$, Mg Ib $\lambda\lambda 5167, 5173, 5184$ triplet, and Ca II $\lambda\lambda 8498, 8542, 8662$ triplet, etc.), σ_* can be measured by matching the observed spectra with the combination of different stellar template spectra broadened by a Gaussian kernel (e.g. Kauffmann et al. 2003; Cid Fernandes et al. 2004; Vanden Berk et al 2006; Greene & Ho 2006b; Zhou et al. 2006; Bian et al. 2006). The SMBH mass can then be estimated from the $M_{\text{bh}} - \sigma_*$ relation if σ_* can be accurately measured from the spectrum of AGN host galaxy.

Here we briefly introduce the method to measure σ_* . Adopting the stellar library from Bruzual & Charlot (2003), we used the stellar population synthesis code, STARLIGHT, (Cid Fernandes et al. 2004, 2005; Bian et al. 2006) to model the observed spectrum O_λ . It models the spectrum M_λ by the linear combination of simple stellar populations (SSP). The model spectrum M_λ is:

$$M_\lambda(x, M_{\lambda_0}, A_V, v_*, \sigma_*) = M_{\lambda_0} \left[\sum_{j=1}^{N_*} x_j b_{j,\lambda} r_\lambda \right] \otimes G(v_*, \sigma_*) \quad (1)$$

where $b_{j,\lambda} \equiv L_\lambda^{\text{SSP}}(t_j, Z_j) / L_{\lambda_0}^{\text{SSP}}(t_j, Z_j)$ is the j^{th} template normalized at λ_0 , x is the population vector, M_{λ_0} is the synthetic flux at the normalization wavelength, r_λ is the reddening term, A_V is the V-band extinction, and $G(v_*, \sigma_*)$ is the line-of-sight stellar velocity distribution, modelled as a Gaussian centered at velocity v_* and broadened by σ_* . The best fit is reached by minimizing χ^2 ,

$$\chi^2(x, M_{\lambda_0}, A_V, v_*, \sigma_*) = \sum_{\lambda=1}^{N_\lambda} [(O_\lambda - M_\lambda) w_\lambda]^2 \quad (2)$$

where the weighted spectrum w_λ is defined as the inverse of the noise in observed spectra. We can obtained some parameters including σ_* by modelling the observed spectrum, which are important for our understanding the stellar populations in AGNs host galaxies.

We download 110 double-peaked spectra from SDSS DR5⁴ in the sample of Strateva et al. (2003), as well as the extinction values at g band. We perform the Galactic extinction correction to observed spectra by using the extinction law of Cardelli, Clayton & Mathis (1989). Then, the rest-frame spectra with errors and masks are obtained by use of the redshift given in their SDSS FITS headers. We normalize the spectra at 4020 Å and the signal-to-noise ratio (S/N) is measured between 4010 and 4060 Å. An additional power-law component is used to represent the AGNs continuum emission. We check visually our modelled spectra sorted by the equivalent width (EW) of CaII K $\lambda 3934$ line. It is found that the fitting goodness depends on the S/N ($\gtrsim 5$), the absorption lines equivalent widths (EW (CaII K) $\gtrsim 1.5$ Å), and the contribution of stellar lights (see also Zhou et al. 2006). At last, 54 double-peaked AGNs are selected, which are well fitted to derive reliable σ_* from their significant stellar absorption. Using the two sample Kolmogorov-Smirnov (K-S) test, *kolmov* task in IRAF, the distributions of the

⁴ <http://cas.sdss.org/dr5/en/tools/search/>

luminosity at 5100\AA in the total sample of Strateva et al. (2003) and our sub-sample are drawn from the same parent population with the probability of 53%. Therefore, this sub-sample is representative of the total sample of Strateva et al. (2003) with respect to the luminosity at 5100\AA . Fig. 1 shows a fitting example for SDSS J082113.71+350305.02. The final results are presented in Table 1, arranging in order of increasing right ascension.

Using Interactive Data Language (IDL), we also carefully model the profiles of [O III] and H β lines. Since the double-peaked profile of the H β line and the asymmetric profiles of [O III] $\lambda\lambda 4959, 5007$ lines, seven-gaussian profiles are used to model these lines carefully, two broad and one narrow components for H β plus two sets of one broad and one narrow components for [O III] $\lambda\lambda 4959, 5007$. We take the same linewidth for each component of [O III] $\lambda\lambda 4959, 5007$, fix the flux ratio of [O III] $\lambda 4959$ to [O III] $\lambda 5007$ to be 1:3, and set their wavelength separation to the laboratory value. And we also set the wavelength separation between the narrow component of H β and the narrow [O III] $\lambda 5007$ to the laboratory value. We do the lines fitting for these 54 stellar-light subtracted spectra. For spectra without obvious stellar features, we do the emission lines fitting for the extinction-corrected rest-frame SDSS spectra without stellar-light subtraction. At last we obtain the gaseous velocity dispersion, σ_g , from the core [O III] $\lambda 5007$ line, the total flux of [O III] $\lambda 5007$ line and the monochromatic flux at 5100\AA . Our emission-line profile fitting for SDSS J022014.57-072859.30 is shown in Fig. 2.

4. THE MASSES AND THE EDDINGTON RATIOS

4.1. The stellar velocity dispersions

In the synthesis, we focus on the strongest stellar absorption features, such as CaII K, G-band, and Ca II $\lambda\lambda$ 8498, 8542, 8662 triplet, which are less affected by emission lines. We put twice more weight for these features during the stellar population synthesis. After correcting the template and the SDSS instrumental resolution, we obtain the value of σ_* through the direct-fitting method.

Cid Fernandes et al. (2005) applied the same synthesis method to a larger sample of 50,362 normal galaxies from the SDSS Data Release 2 (DR2). Their σ_* is consistent very well with that of the MPA/JHU group (Kauffmann et al. 2003), the median of the difference is just 9 km s^{-1} . They also gave the σ_* uncertainty based on the S/N (see Table 1 in Cid Fernandes et al. 2005). Typically, the σ_* uncertainty based on S/N at 4020\AA is about: 24 km s^{-1} at S/N=5; 12 km s^{-1} at S/N=10; 8 km s^{-1} at S/N=15. In order to use the typical errors suggested by Cid Fernandes et al. (2005), we calculate the S/N and the starlight fraction at 4020\AA . The S/N is the mean flux divided by the root mean square (RMS) of the flux in the range 4010 to 4060\AA . We also performed the method of Cid Fernandes et al. (2005) to compute the S/N by using the SDSS error spectrum, the results are almost the same. Considering the contribution from featureless continuum (FC, represented by a power law), we use an effective S/N to show the typical error of σ_* , where the effective S/N is roughly the S/N multiplied by the stellar fraction. We use the featureless continuum fraction as the up limit of nuclei contribution, because the fea-

tureless continuum can be attributed either by a young dusty starburst, by an AGN, or by these two combination (Cid Fernandes et al. 2004). Therefore, the effective S/N is the low limit. In our sample, the effective mean spectral S/N at 4020\AA for these objects are 7.2 (see Table 1). Thus the typical uncertainty in σ_* should be around 20 km s^{-1} . For 13 objects with effective S/N less than 5, their σ_* in Table 1 are preceded by colons.

Here, we also apply this synthesis method to a sample of the local AGNs presented by Greene & Ho (2006a). Greene & Ho (2006a; 2006b) performed a research on the systematic bias of σ_* derived from the regions around CaII triplet, MgIb triplet, and CaII H+K, respectively (Barth et al. 2002). They argued that the CaII triplet provide the most reliable measurements of σ_* and there is a systematic offset between σ_* from CaII K line and that from other spectral regions. We use our synthesis method to their sample in two manners: one is using whole spectrum, the other is just using partial spectrum between 3200\AA and 7500\AA at the rest frame. We put twice more weight for the strongest absorption features of Ca H+K $\lambda\lambda$ 3969, 3934, G-band, and Ca II $\lambda\lambda$ 8498, 8542, 8662 triplet. We find that the values of σ_* in these two manners are similar by performing our synthesis method. By using the least-square regression, the best fit between the σ_* from these two manners (σ_*^{whole} and $\sigma_*^{\text{partial}}$, respectively) is: $\sigma_*^{\text{whole}} = (5.49 \pm 3.29) + (0.95 \pm 0.03)\sigma_*^{\text{partial}}$. The spearman coefficient R is 0.97, with a probability of $p_{\text{null}} < 10^{-4}$ for rejecting the null hypothesis of no correlation.

Because the SDSS spectral coverage is from 3800\AA to 9200\AA , most of double-peaked AGNs with redshift larger than 0.083 will not cover the range of CaII triplet. For those sources with redshift larger than 0.083, we used the above formula to obtain the corrected velocity dispersion, i.e. $\sigma_*^c = (5.49 \pm 3.29) + (0.95 \pm 0.03) \times \sigma_*$. The corrected velocity dispersion is listed in Col. (8) in Table 1. And we find that the corrected velocity dispersion is almost the same to the uncorrected one. The largest difference is about 10 km s^{-1} , which is less than the typical error of 20 km s^{-1} .

Based on the SDSS instrumental resolution, we take 60 km s^{-1} as a lower limit of σ_* (e.g. Bernardi 2003). Only for two objects, SDSS J133433.24 -013825.41 and SDSS J214555.03 +121034.17, the measured σ_* are below/near the lower limit (51 km s^{-1} and 62 km s^{-1} , respectively). These two objects are excluded from further analysis.

The σ_* value from the partial SDSS spectra is also used to compare our result with Greene & Ho (2006a), who fitted the region around CaII triplet directly. In Fig. 3, we compared our σ_* with theirs. We found that the agreement is quite good, the σ_* difference ($\sigma_*^{\text{GH}} - \sigma_*^{\text{partial}}$) distribution is -2.1 km s^{-1} with a standard deviation (SD) of 22.7 km s^{-1} . By using the least-square regression considering the errors of σ_*^{GH} , the best fit between σ_*^{GH} and $\sigma_*^{\text{partial}}$ is: $\sigma_*^{\text{GH}} = (-16.66 \pm 3.56) + (1.09 \pm 0.04)\sigma_*^{\text{partial}}$ (solid line in Fig. 3). The spearman coefficient R is 0.86, the standard deviation is 2.11, with $p_{\text{null}} < 10^{-4}$.

4.2. The Results

For these double-peaked AGNs with reliable σ_*^c , we use the $M_{\text{bh}} - \sigma_*$ relation to derive the SMBH mass (e.g.

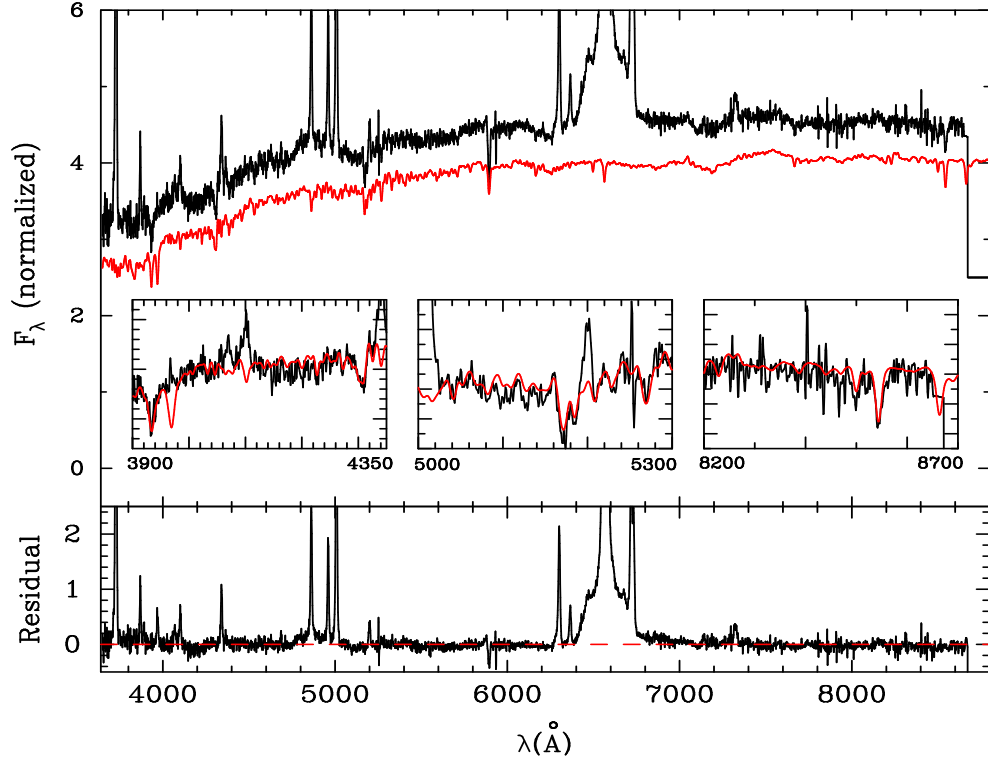


FIG. 1.— Sample fit of the synthetic population model for SDSS J081700.40+34556.34. The top panel is the logarithm of the observed spectrum (top black curve) and the synthetic spectra (bottom red curve)(shifted down for clarity). In this top panel, we also show the region around Ca H+K $\lambda\lambda$ 3969, 3934 and G-band (left); the region around Mg Ib $\lambda\lambda$ 5167, 5173, 5184 triplet, Fe 5270 \AA (middle); the region around Ca II $\lambda\lambda$ 8498, 8542, 8662 triplet (right). The residual spectrum is shown in the bottom panel.

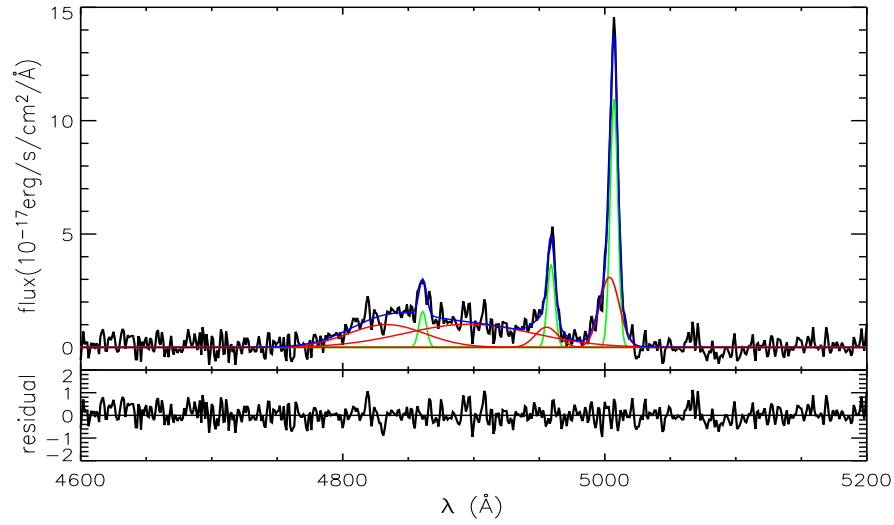


FIG. 2.— Sample multi-component fitting of the [O III] $\lambda\lambda$ 4959, 5007 lines for SDSS J022014.57-072859.30: composite profile(blue curves); narrow components (green curves); broad components (red curves); the residue (bottom panel).

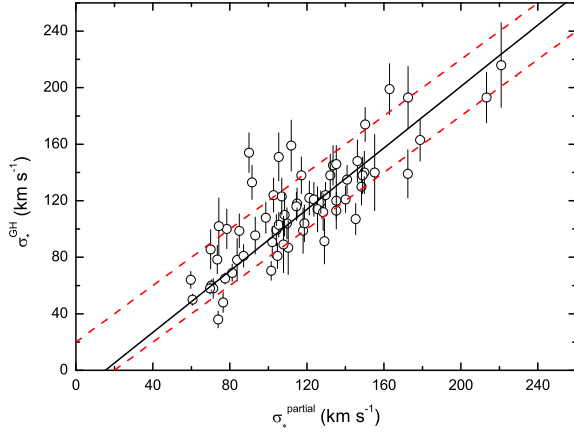


FIG. 3.— Comparison of our σ_* from the partial SDSS spectra with that for a sample of the local AGNs presented by Greene & Ho (2006a). The solid line denotes our best linear fit, the red dash lines are $y = x \pm 20 \text{ km s}^{-1}$. Considering the error bar of σ_* presented by Greene & Ho (2006a), most of local AGNs are located between two red dash lines.

Tremaine et al. 2002 and reference therein),

$$M_{\text{bh}}(\sigma_*^c) = 10^{8.13} \left(\frac{\sigma_*^c}{200 \text{ km s}^{-1}} \right)^{4.02} M_{\odot}. \quad (3)$$

We calculate the Eddington ratio, e.g., the ratio of the bolometric luminosity (L_{bol}) to the Eddington luminosity (L_{Edd}), where $L_{\text{Edd}} = 1.26 \times 10^{38} (M_{\text{bh}}/M_{\odot}) \text{ erg s}^{-1}$. We use the monochromatic luminosity at 5100Å (λL_{λ} at 5100Å) to estimate the bolometric luminosity, $L_{\text{bol}} = c_B \lambda L_{\lambda}(5100\text{Å})$, where $c_B = 9$ (Kaspi et al. 2000). These results are presented in Table 1.

For the typical uncertainty of 20 km s^{-1} for $\sigma_* = 200 \text{ km s}^{-1}$, the error of $\log \sigma_*$ would be about 0.05 dex, corresponding to 0.2 dex for $\log M_{\text{bh}}$. The error of $\log M_{\text{bh}}$ is about 0.4 considering the error of 0.3 dex from the $M_{\text{bh}} - \sigma_*$ relation (Tremaine et al. 2002). Richards et al. (2006) suggested a bolometric correction factor of 10.3 ± 2.1 at 5100 Å. Therefore, the final Eddington ratio, $L_{\text{bol}}/L_{\text{Edd}}$, has a large uncertainty, about 0.5 dex.

In Fig. 4, we show the histograms of the black hole masses and the accretion ratios for these 52 double-peaked AGNs. The black hole masses range from 1.0×10^7 to $5.5 \times 10^8 M_{\odot}$ with a mean value of $\log M_{\text{bh}}/M_{\odot} = 7.76 \pm 0.37$. Using the $\text{H}\alpha$ FWHM and the 5100Å monochromatic luminosity, Wu & Liu (2004) estimated the SMBH masses and the Eddington ratios for an assembled double-peaked AGNs sample. Lewis & Eracleous (2006) noted that the BH masses from the $\text{H}\alpha$ FWHM are not completely consistent with those from the stellar velocity dispersion. Our BH masses derived from σ_*^c are indeed smaller than those from the $\text{H}\alpha$ FWHM (Wu & Liu 2004) by about an order of magnitude. This will lead to our $L_{\text{bol}}/L_{\text{Edd}}$ larger than that from the $\text{H}\alpha$ FWHM by almost an order of magnitude.

The Eddington ratio has a distribution with mean and the standard deviation of $\log(L_{\text{bol}}/L_{\text{Edd}})$ is -1.13 ± 0.38 .

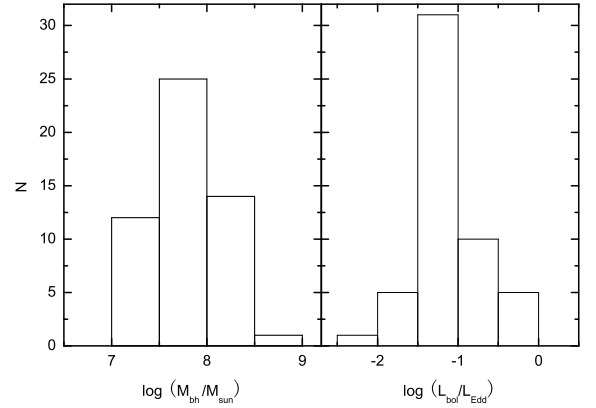


FIG. 4.— The histograms of the black hole masses (left) and the Eddington ratios (right) for these 52 double-peaked AGNs with reliable σ_*^c .

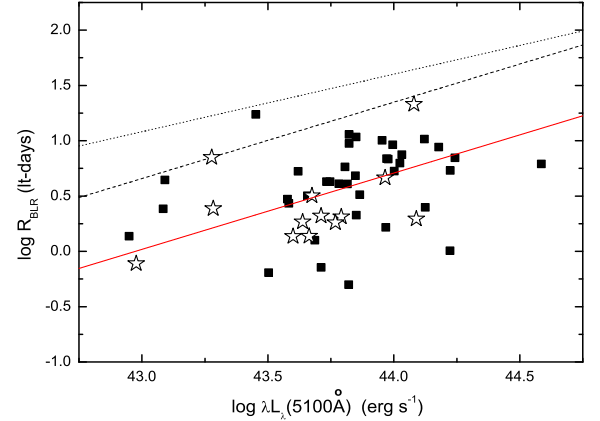


FIG. 5.— The BLRs sizes versus the monochromatic luminosity at 5100Å (where $f=0.75$ for random BLRs orbits). Objects with effective S/N in 4020 Å less than 5 is denoted as open stars. The black dash line is the empirical size-luminosity relation, $R_{\text{BLR}} = 22.3 \times [\lambda L_{\lambda}(5100\text{Å})/10^{44} \text{ ergs}^{-1}]^{0.69} \text{ lt-days}$, found by Kaspi et al. (2005). The black dot line is the empirical size-luminosity relation, $R_{\text{BLR}} = 40 \times (\lambda L_{\lambda}(5100\text{Å})/10^{44} \text{ ergs}^{-1})^{0.52} \text{ lt-days}$, found by Bentz et al. (2006). The red solid line is our best fit with the fixed slope of 0.69 ($R=0.29$), lower by -0.63 dex respect to dash line.

It is suggested that the accretion disk in double-peaked AGNs is in the mode of Advection Dominated Accretion Flow (ADAF) (e.g. Eracleous & Halpern 2003). When the Eddington ratio is below than the critical one $L_{\text{bol}}/L_{\text{Edd}} \sim 0.0028 \alpha_{0.1}^2$ (Mahadevan 1997), the ADAF appears, where $\alpha_{0.1} = \alpha/0.1$ is viscous coefficient. For our SDSS sample, all objects have Eddington ratios larger than this critical value of 0.0028. The present results from Fig. 4 clearly show that these double peaked AGNs have accretion disks in the standard regime.

The black hole masses can be independently tested by the relation between the black holes and bulges. The Appendix gives details of the test. We find the black hole masses are consistent from $M_{\text{bh}} - M_{\text{bulge}}$ and $M_{\text{bh}} - \sigma_*$ relations.

5. BLRS IN DOUBLE-PEAKED AGNS

5.1. The size of BLRs

We also calculate the BLRs sizes for these 52 double-peaked AGNs using the SMBHs masses derived from σ_*^c and the $\text{H}\alpha$ FWHM. We firstly transform the $\text{H}\alpha$ FWHM to the $\text{H}\beta$ FWHM by (Greene & Ho 2005b):

$$\text{FWHM}_{\text{H}\beta} = (1.07 \pm 0.07) \times 10^3 \left(\frac{\text{FWHM}_{\text{H}\alpha}}{10^3 \text{ kms}^{-1}} \right)^{(1.03 \pm 0.03)} \text{ kms}^{-1} \quad (4)$$

From the SMBH masses derived from the velocity dispersions, we can calculate the BLRs sizes:

$$R_{\text{BLR}} = \frac{M_{\text{bh}}(\sigma_*^c) \times 5.123}{f \times \text{FWHM}_{\text{H}\beta}^2} \text{ lt-days}, \quad (5)$$

where f is the scaling factor related to the kinematics and geometry of the BLRs, defined by $M_{\text{bh}} = f \frac{R_{\text{BLR}} V_p^2}{G}$, V_p is the Keplerian velocity in disk plane. For random orientation of BLR cloud Keplerian orbits, f is 0.75.

In Fig. 5, we plot the BLRs sizes versus the monochromatic luminosity at 5100\AA (assuming $f=0.75$ for random BLRs orbits). Almost all objects are located below the empirical size-luminosity relation (black dash line) found by Kaspi et al. (2005). The correlation between the BLRs sizes and the monochromatic luminosity at 5100\AA is not too strong. The best fit is shown as red solid line in Fig. 5 as $R_{\text{BLR}} = 5.1 [\lambda L_\lambda(5100\text{\AA})/10^{44} \text{ ergs}^{-1}]^{0.69}$ lt-days ($R = 0.34$, $P_{\text{null}} = 0.20$), lower by -0.64 dex respecting to the empirical relation found by Kaspi et al. (2005). When excluding objects with effective S/N in 4020\AA less than 5 (open stars in Fig. 5), for fixed slope of 0.69, the best fit gives almost the same line but with a smaller R of 0.28.

If we used $f=0.52$ (Table 2 in Collin et al. 2006), $\log R$ will increased by 0.16 dex, the BLRs sizes of double-peaked AGNs are still deviated from the empirical relation found by Kaspi et al. (2005) (about 0.48 dex). FWHMs of the double-peaked AGNs are about twice as broad as other AGN of similar luminosity (Eracleous & Halpern 1994, 2003; Strateva et al. 2003). If the double-peaked AGNs are not systematically more massive than other AGNs, equation 5 suggested that BLRs radii can be smaller than for a similarly massive "normal" AGNs by a factor of 4.

We have to point out that here we are not really testing the $R_{\text{BLR}} - L$ relation in double peaked AGNs, but the comparison with $R_{\text{BLR}} - L$ relation allows us to derive the factor f .

5.2. The factor f , BLR inclinations and Non-virial BLRs

If we use the empirical $R_{\text{BLR}} - L$ relation (Kaspi et al. 2005) to derive the R_{BLR} and the SMBH masses, $M_{\text{bh}}(\sigma_*^c)$, to do the calibration of the factor f (Onken et al. 2004), we find that the distribution of f is 0.179 with

a standard deviation of 0.171. It is not consistent with the value of $\langle f \rangle = 5.5/4$ presented by Onken et al. (2004) and it is about $1/3$ of 0.52 ± 0.13 suggested by Collin et al. (2006). Our results suggest that the empirical relation between the BLRs sizes and the luminosity at 5100\AA does not hold for double-peaked AGNs (see also Zhang et al. 2007), otherwise the calibration factor f should be as low as 0.179. An important consequence of the breakdown in the size-luminosity relationship is that using mass estimation methods based on the size-luminosity relationship and the calibration factor of 0.75 can lead to an order of magnitude over-estimate of the SMBH mass (Wu & Liu 2004).

If BLRs are disk-like with an inclination of θ , the relation between the $\text{H}\beta$ FWHM and the Keplerian disk plane velocity, v_p , is given by (Wills & Browne 1986)

$$\text{FWHM}_{\text{H}\beta} = 2 (V_r^2 + V_p^2 \sin^2 \theta)^{1/2}, \quad (6)$$

where V_r is the random isotropic component. We may derive the scaling factor as $f = 1/[4(V_r/V_p)^2 + 4\sin^2 \theta]$. Ignoring V_r , $f = 1/(2\sin^2 \theta)^2$, and the minimum of f is 0.25. For only ten object with $f > 0.25$, we can derive the inclination of θ by the above formula. The mean inclination is 56 degrees. It is suggested that double-peaked AGNs are not preferentially edge-on (Eracleous & Halpern 1994, 2003; Strateva et al. 2003), most have an inclination of less than 50 degrees. If all these objects were nearly edge-on, the obscuring torus would prevent us from seeing the broad lines. Collin et al. (2006) suggested that objects with large FWHMs, inclination effects are not really important. In these 52 double-peaked AGNs, 42 objects have smaller f less than 0.25. V_r can't be omitted, we need to consider the random isotropic component, implying the non-virial dynamics of BLRs in double-peaked AGNs. If we use f to trace the non-virial effect, smaller f means strong non-virial effect. We find f have strong correlations with $\log M_{\text{bh}}$ and $\log(L_{\text{bol}}/L_{\text{Edd}})$ (see Fig. 6). Using the least-square regression, we derive the correlations are:

$$\log f = (-1.63 \pm 0.12) - (0.65 \pm 0.10) \log(L_{\text{bol}}/L_{\text{Edd}}), \quad (7)$$

where $R = -0.69$, $p_{\text{null}} < 10^{-4}$; and

$$\log f = (-4.31 \pm 0.97) + (0.44 \pm 0.13) \log M_{\text{bh}}/M_\odot, \quad (8)$$

where $R = 0.45$ with $p_{\text{null}} = 9.6 \times 10^{-4}$. When we exclude objects with effective S/N in 4020\AA less than 5 (open stars in Fig. 6), the best fits for f relations between SMBH mass and the Eddington ratio give a little larger R ($-0.75, 0.52$, respectively). We should note that the reason of these strong correlations are that f is derived from M_{bh} , R_{BLR} [from $\lambda L_\lambda(5100\text{\AA})$], and $\text{FWHM}_{\text{H}\beta}$. These strong correlations suggest that objects with larger Eddington ratios have strong non-virial effect.

3C 390.3 is the only double peaked object with the direct measurements of the time delay and the host stellar velocity dispersion. And it locates in the empirical relation between BLRs sizes and the luminosity (e.g. Kaspi et al. 2005). By σ_* of 240 km s^{-1} (Onken et al. 2004), we find that f is about 1.3, consistent with the assumption of random BLRs orbits in 3C390.3. Its small Eddington ratio (Lewis & Eracleous 2006), $(2 - 4) \times 10^{-2}$, is also consistent with the virial BLRs dynamics (See Fig. 6).

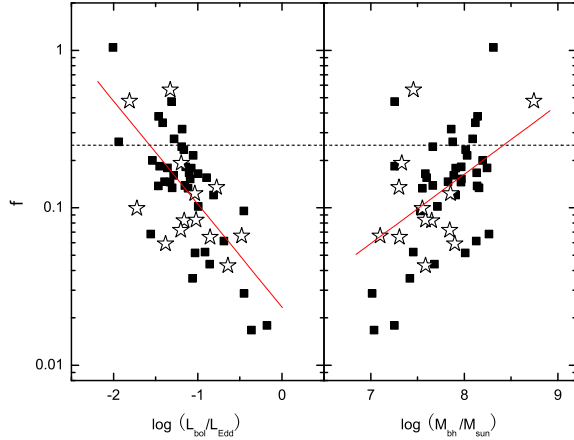


FIG. 6.— The scaling factor f versus the Eddington ratio (left panel) and the SMBH masses (right panel). Objects with effective S/N in 4020 Å less than 5 is denoted as open stars. The dash lines are $f = 0.25$. The correlation coefficient for the relation between the peak separation and the Eddington ratio is $R = -0.69$ and that between the separation and the black hole mass is $R = 0.45$.

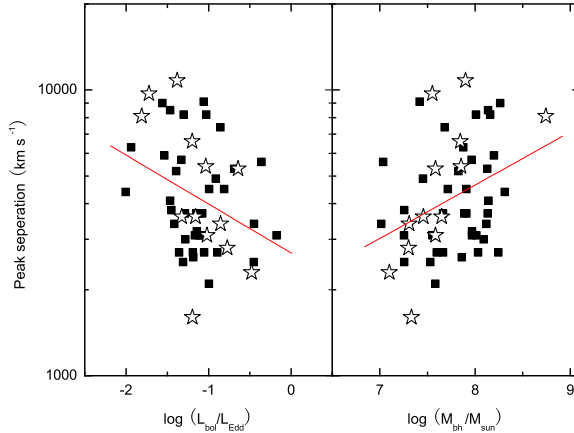


FIG. 7.— The peak separation versus the Eddington ratio (left panel) and the SMBH masses (right panel). Objects with effective S/N in 4020 Å less than 5 is denoted as open stars. The correlation coefficient for the relation between the peak separation and the Eddington ratio is $R = -0.33$, which is almost the same for that between the separation and the black hole mass ($R = 0.35$).

6. PEAK SEPARATION, BH MASS AND EDDINGTON RATIO

For double-peaked AGNs, the peak separation, $\Delta v = \lambda_{\text{red}} - \lambda_{\text{blue}}$, has a large variance ranging from about 1000 km s⁻¹ to about 10000 km s⁻¹ (Table 3 in Strateva et al. 2003). In Fig. 7, we show the relations between $\log \Delta \lambda$ and $\log(L_{\text{bol}}/L_{\text{Edd}})$, $\log M_{\text{bh}}$. Using the least-square regression, we derive the correlation between $\log \Delta v$ and

$\log(L_{\text{bol}}/L_{\text{Edd}})$ to be:

$$\log \Delta v = (3.43 \pm 0.08) - (0.17 \pm 0.06) \log(L_{\text{bol}}/L_{\text{Edd}}), \quad (9)$$

where $R = -0.33$, $p_{\text{null}} = 0.017$ (see Fig. 7). For the relation between $\log \Delta \lambda$ and $\log M_{\text{bh}}$,

$$\log \Delta v = (2.17 \pm 0.55) + (0.11 \pm 0.08) \log(M_{\text{bh}}/M_{\odot}), \quad (10)$$

where R is 0.35 with $p_{\text{null}} = 0.011$. When excluding objects with effective S/N in 4020 Å less than 5 (open stars in Fig. 7), the best fits for $\log \Delta v$ relations between SMBH mass and the Eddington ratio give smaller R ($-0.22, 0.21$, respectively). We also do the multiple regression for the dependence of Δv on $\log(L_{\text{bol}}/L_{\text{Edd}})$ and $\log M_{\text{bh}}$,

$$\log \Delta v = (2.54 \pm 0.64) + (0.13 \pm 0.09) \log(M_{\text{bh}}/M_{\odot}) - (0.10 \pm 0.09) \log(L_{\text{bol}}/L_{\text{Edd}}), \quad (11)$$

where the R -Square correlation coefficient is 0.15.

Wu & Liu (2004) also studied this correlation and obtained an apparent stronger correlation ($R = 0.84$). Their derived strong correlation is mainly due to the very strong correlation between the separation and the H α FWHM ($R = 0.88$). When the H α FWHM is fixed, they found that the partial correlation coefficient is only 0.05. In this paper, we use the stellar velocity dispersion to estimate the black hole masses, and we also find a mild correlation between Δv and $L_{\text{bol}}/L_{\text{Edd}}$, which implies that the peak separation would be smaller for AGNs with higher Eddington ratios. It provides clues to why previous double-peaked AGNs have lower Eddington ratios.

There is increasing evidence for a disk geometry of the BLR (see a review of Laor 2007). If we assume that peak separation is created by the doppler shift of the movement of a thin annulus and the annulus radius corresponds the location where the self-gravitation dominates (Bian & Zhao 2002), we have the radius $R_{\text{SG}}/R_g = 3586 m_8^{-2/9} \dot{m}^{4/9} \alpha^{2/9}$ (their eq. 18 in Laor & Netzer 1989), where $R_g = 1.5 \times 10^{13} m_8$ cm, $m_8 = M_{\text{bh}}/10^8 M_{\odot}$, \dot{m} is the Eddington ratio and α is the viscosity. The maximum separation of the double peaks in units of Å under the edge-on orientation to an observer is given

$$\Delta \lambda = \lambda_0 \left(\frac{R_g}{R_{\text{SG}}} \right)^{1/2} = 84.9 \alpha_{0.1}^{-1/9} \dot{m}^{-2/9} m_8^{1/9} \text{ Å}, \quad (12)$$

where we use the peak separation in term of separation velocity,

$$\Delta v = 7.76 \times 10^3 \alpha_{0.1}^{-1/9} \dot{m}^{-2/9} m_8^{1/9} \text{ km s}^{-1}. \quad (13)$$

where $\alpha_{0.1} = \alpha/0.1$ and H α wavelength $\lambda_0 = 6563 \text{ Å}$.

Considering the uncertainties of the fitting results for the peak separation correlations with SMBH mass and the Eddington ratio, the slopes are consistent with the simple theoretical expectation. We have to stress that equation (11) is for the maximum separation (edge-on orientation) when the disk structure is given. More sophisticated model is needed for explanations of the dependence of peak separations and Eddington ratios. The scatters in Fig 7 may be caused by different orientation of the BLR in the sample.

We also find no significant correlations between the ratio of the red peak height to the blue height and the Eddington ratio, the black hole mass, the peak separation. Since the Keplerian velocity is much below the light speed, the Doppler boosting effects could be hidden by complex situations of the BLR.

7. ENERGY BUDGET

Here we discuss the energy budget of the line-emitting accretion disk. Based on the standard accretion disk model, the disk radiation as a function of radius ξ is (Chen et al. 1989):

$$F(\xi) = 1 \times 10^{12} m_8^{-2} \dot{M}_{24} \xi_{100}^{-3} [1 - (6/\xi)^{1/2}] \text{ ergs cm}^{-2} \text{ s}^{-1} \quad (14)$$

where $m_8 = M_{\text{bh}}/10^8 M_\odot$, \dot{M}_{24} is the accretion rate in units of $10^{24} g \text{ s}^{-1}$, and the dimensionless radius ξ_{100} is $\xi/(100 R_g)$. Using $\dot{M} = L_{\text{bol}}/(\zeta c^2)$ where the efficiency ζ is 0.1, the gravitational power output of the line-emitting disk annulus between ξ_1 and ξ_2 is (Eracleous & Halpern 1994):

$$W_{\text{disk}}(\xi_1, \xi_2) = 7.7 \times L_{\text{bol}} \left[\frac{1}{\xi_1} \left(1 - \sqrt{\frac{8}{3\xi_1}} \right) - \frac{1}{\xi_2} \left(1 - \sqrt{\frac{8}{3\xi_2}} \right) \right] \text{ ergs s}^{-1}, \quad (15)$$

where L_{bol} is in units of erg s^{-1} . It is noted that W_{disk} is independent of the black hole mass, when we use the typical radius in units of R_g . We use the luminosity at 5100\AA to calculate the bolometric luminosity. From the work of Eracleous & Halpern (2003) and Strateva et al. (2003), the inner radius is about hundreds of R_g , and the outer radius is about thousands of R_g . The outer radius of line-emitting accretion disk is about near the inner position of torus. We can assume typical inner and outer radii of $\xi_1 = 450 R_g$ and $\xi_2 = 3000 R_g$ to calculate the energy output for these double-peaked SDSS AGNs, i.e. $W_{\text{disk}} = 10^{-1.876} \times L_{\text{bol}} \text{ erg s}^{-1}$. The distribution of $\log(L_{\text{H}\alpha}/W_{\text{disk}})$ is -0.55 ± 0.06 with the standard deviation of 0.57 (see also Fig. 8). If assuming as much as 20% of the power was radiated as H α line (dashed line in Fig. 8), our results show that only 36 out of 105 double-peaked AGNs would generate enough power to produce observed strength of H α emission. If we adopt the value of 10%, more objects (83 out of 105 objects) showed the energy problem. It implied that the majority of double-peaked AGNs need external illumination of the disk (e.g. an inner iron torus or corona) to produce the observed strength of H α line (Strateva et al. 2006; Cao & Wang 2006).

8. CONCLUSIONS

We use the simple population synthesis to model the stellar contributions in double-peaked SDSS AGNs. The reliable stellar velocity dispersions are obtained for 52 medium-luminous double-peaked SDSS AGNs with obvious stellar features. We find that: 1) The black hole mass is from $1.0 \times 10^7 M_\odot$ to $5.5 \times 10^8 M_\odot$ and the Eddington ratio is from about 0.01 to about 1; 2) The factor f far deviates from the virialized value 0.75, suggesting the non-virial dynamics of BLRs; 3) The peak separation is mildly correlated with the Eddington ratio and SMBH mass with almost the same correlation coefficients, which

can be interpreted in the doppler shift of thin annulus of BLRs created by gravitational instability; 4) Based on the line-emitting accretion disk model, we need external illumination of the accretion disk to produce the observed strength of H α line. In the future, using different models, we would fit the double-peaked profiles to constrain the nature of double-peaked AGNs. We can also use the double-peaked AGNs to constrain the BLRs origin (Nicastro 2000; Laor 2003; Bian & Gu 2007).

ACKNOWLEDGMENTS

We are very grateful to the anonymous referee and Ari Laor for their thoughtful and instructive comments which significantly improved the content of the paper. We thank Luis C. Ho for his very useful comments, and thank discussions among people in IHEP AGN group. This work has been supported by the NSFC (Nos. 10403005, 10473005), the Science-Technology Key Foundation from Education Department of P. R. China (No. 206053), and and the China Postdoctoral Science Foundation (No. 20060400502). QSG would like to acknowledge the financial supports from China Scholarship Council (CSC) and the NSFC under grants 10221001 and 10633040. JMW thanks NSFC grants via No. 10325313 and 10521001 and supports from CAS key project via KJCX2-YW-T03.

Funding for the SDSS and SDSS-II has been provided by the Alfred P. Sloan Foundation, the Participating Institutions, the National Science Foundation, the U.S. Department of Energy, the National Aeronautics and Space Administration, the Japanese Monbukagakusho, the Max Planck Society, and the Higher Education Funding Council for England. The SDSS is managed by the Astrophysical Research Consortium for the Participating Institutions. The Participating Institutions are the American Museum of Natural History, Astrophysical Institute Potsdam, University of Basel, Cambridge University, Case Western Reserve University, University of Chicago, Drexel University, Fermilab, the Institute for Advanced Study, the Japan Participation Group, Johns Hopkins University, the Joint Institute for Nuclear Astrophysics, the Kavli Institute for Particle Astrophysics and Cosmology, the Korean Scientist Group, the Chinese Academy of Sciences (LAMOST), Los Alamos National Laboratory, the Max-Planck-Institute for Astronomy (MPIA), the Max-Planck-Institute for Astrophysics (MPA), New Mexico State University, Ohio State University, University of Pittsburgh, University of Portsmouth, Princeton University, the United States Naval Observatory, and the University of Washington.

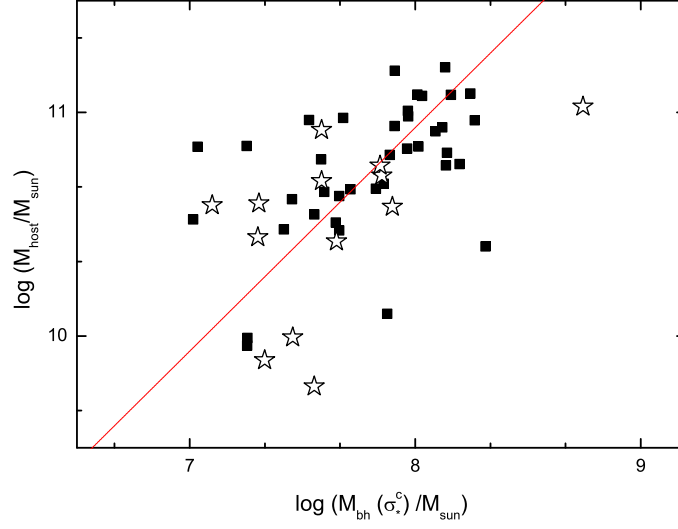


FIG. 9.— The relation between the host mass and the SMBH mass. With fixed slope of 1, the solid line denotes the best fit with $R=0.53$ and $p_{\text{null}} < 10^{-4}$. Objects with effective S/N in 4020 Å less than 5 is denoted as open stars.

APPENDIX

THE RELATION BETWEEN THE HOST MASS AND THE SMBH MASS

For the sample of 52 double-peaked SDSS AGNs, assuming $\lambda L_{\lambda} \propto \lambda^{0.5}$, $\lambda L_{\lambda}(5100\text{\AA})$ is translated to $\lambda L_{\lambda}(5530\text{\AA})$. The host luminosity in V band is the value of $\lambda L_{\lambda}(5530\text{\AA})$ multiplied by the stellar fraction at 5530Å. We assume that the host luminosity in V band approximates the bulge luminosity L_{bulge} in V-band. We then use the following formula to calculate the bulge mass: $\log(M_{\text{bulge}}/M_{\odot}) = 1.18 \log(L_{\text{bulge}}/L_{\odot}) - 1.11$ (Magorrian et al. 1998). Fig. 9 shows this bulge mass versus the BH mass from σ_* . We fit with fixed slope as 1, intercept is 2.93 ± 0.05 , correlation coefficient is 0.53. The null hypothesis is less than 10^{-4} . We find that the M_V^{bulge} versus the $\log \sigma$ relation is consistent with Fig. 4 of Faber et al. 1997. Therefore, the SMBH mass from L_{bulge} and the Magorrian relation agrees with that from σ_* . When we exclude objects with effective S/N in 4020 Å less than 5 (open stars in Fig. 9), for fixed slope of 1, the best fit gives that intercept is 2.95 ± 0.05 , correlation coefficient is 0.49.

It is suggested that the mass from the $M_{\text{bh}} - \sigma_*$ relation could underestimate the SMBH mass for the massive ellipticals with SMBH mass larger than $10^9 M_{\odot}$ (Fig. 2 in Lauer et al. 2007). For our 52 double-peaked AGNs, their SMBH masses are all less than $10^9 M_{\odot}$ from $M_{\text{bh}} - M_{\text{bulge}}$ relation. The present results are less affected by Lauer et

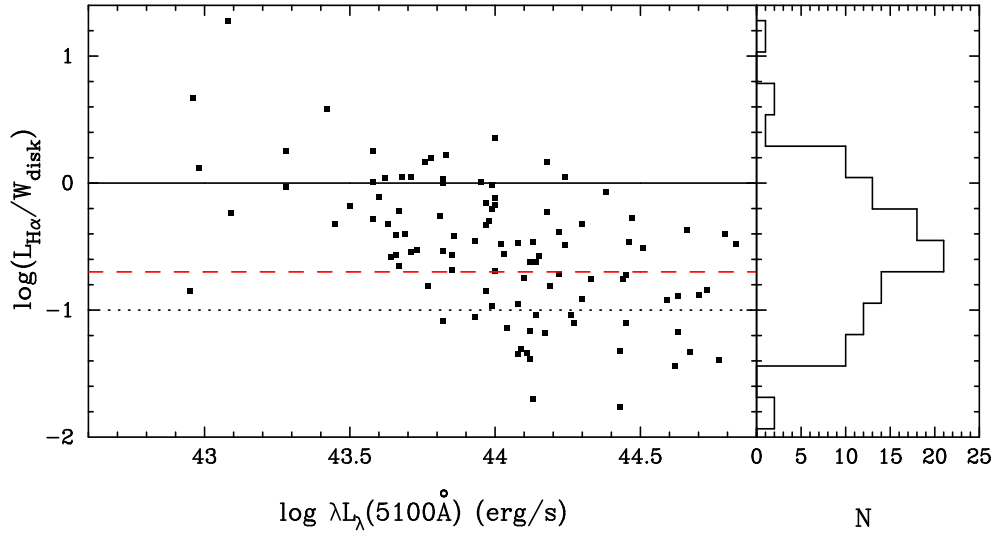


FIG. 8.— The ratio of the $H\alpha$ line luminosity ($L_{H\alpha}$) to the line-emitting power (W_{disk}) versus the monochromatic luminosity at 5100Å ($\log \lambda_{L\lambda}(5100 \text{ \AA})$). The solid line is $L_{H\alpha} = W_{\text{disk}}$, the dash line is $L_{H\alpha} = 0.2W_{\text{disk}}$, and the dot line is $L_{H\alpha} = 0.1W_{\text{disk}}$. We display the histogram of the distribution of $L_{H\alpha}/W_{\text{disk}}$ (right).

al's findings.

REFERENCES

- Abazajian, K., et al. 2005, *AJ*, 129, 1755
 Barth, A. J., Ho, L. C., Filippenko, A. V., Rix, H., Sargent, W. L. W. 2001, *ApJ*, 546, 205
 Bentz et al. 2006, *ApJ*, 644, 133
 Bernardi, M., et al. 2003, *AJ*, 125, 1817
 Bian, W., Zhao, Y. 2002, *A&A*, 395, 465
 Bian, W., Zhao, Y. 2004, *MNRAS*, 347, 607
 Bian, W., Yuan, Q., Zhao, Y. 2005, *MNRAS*, 364, 187
 Bian, W., Gu, Q., Zhao, Y., Chao, L., Cui, Q. 2006, *MNRAS*, 372, 876
 Bian, W., Gu, Q. 2007, *ApJ*, 657, 159
 Bower, G. A., Wilson, A. S., Heckman, T. M., Richstone, D. O. 1996, *AJ*, 111, 1901
 Bruzual, G., Charlot, S. 2003, *MNRAS*, 344, 1000
 Cao, X.W., Wang, T.G. 2006, *ApJ*, 652, 112
 Cardelli, J. A., Clayton, G. C., Mathis, J. S. 1989, *ApJ*, 345, 245
 Chen, K., Halpern, J. P. 1989, *ApJ*, 344, 115
 Cid Fernandes R., Gu Q., Melnick J., et al. 2004, *MNRAS*, 355, 273
 Cid Fernandes R., Mateus A., Sodre L., Stasinska G., Gomes J. 2005, *MNRAS*, 358, 363
 Collin, S. et al. 2006, *A&A*, 456, 75
 Dietrich, M., et al. 1998, *ApJS*, 115, 185
 Eracleous, M., Halpern, J. P. 1994, *ApJS*, 90, 1
 Eracleous, M., Halpern, J. P. 2003, *ApJ*, 599, 886
 Eracleous, M., et al. 1997, *ApJ*, 490, 216
 Gezari, S., Halpern, J. P., Eracleous, M. 2007, *ApJS*, 169, 167
 Goad, M., Wanders, I. 1996, *ApJ*, 469, 113
 Greene, J. E., Ho, L. C. 2005a, *ApJ*, 627, 721
 Greene, J. E., Ho, L. C. 2005b, *ApJ*, 630, 122
 Greene, J. E., Ho, L. C. 2006a, *ApJL*, 641, L21
 Greene, J. E., Ho, L. C. 2006b, *ApJ*, 641, 117
 Grupe, D., Mathur, S. 2004, *ApJ*, 606, L41
 Hao, L., et al. 2003, *AJ*, 129, 1783
 Heckman, T. M., et al. 2004, *ApJ*, 613, 109
 Ho, L. C., Rudnick, G., Rix, H., Shields, J. C., McIntosh, D. H., Filippenko, A. V., Sargent, W. L. W., Eracleous, M. 2000, *ApJ*, 541, 120
 Kaspi, S., Maoz, D., Netzer, H., Peterson, B.M., Vestergaard, M., & Jannuzi, B.T. 2005, *ApJ*, 629, 61
 Kaspi, S., Smith, P.S., Netzer, H., Maoz, D., Jannuzi, B.T., Givon, U. 2000, *ApJ*, 533, 631
 Kauffmann, G., et al. 2003, *MNRAS*, 346, 1055
 Kauffmann, G., Heckman, T. M. 2005, *Philos. Trans. R. Soc. London*, A363, 621
 Lauer, T. R., et al. 2007, *ApJ*, 662, 808
 Laor, A. 2003, *ApJ*, 590, 86
 Laor, A. 2007, in *Proceedings of The Central Engine of Active Galactic Nuclei*, ed. L. C. Ho & J.-M. Wang (San Francisco: ASP) in press (astro-ph/0702577)
 Laor, A. & Netzer, H. 1989, *MNRAS*, 238, 897
 Kormendy, J., & Gebhardt, K. 2001, in *Proc. 20th Texas Symposium*, ed. H. Martel & J. C. Wheeler (Austin: AIP), 363
 Krolik, J. H. 2001, *ApJ*, 551, 72
 Lewis, K. T., Eracleous, M. 2006, *ApJ*, 642, 711
 Lewis, K. T. 2006, In *ASP Conference Series*, the central engine of Active galactic Nuclei.
 Mahadevan, R. 1997, *ApJ*, 477, 585
 Magorrian, J., et al. 1998, *AJ*, 115, 2285
 Mathur, S., Kuraszewicz, J., Czerny, B. 2001, *NewA*, 6, 321
 McLure, R. J., Jarvis, M. J. 2002, *MNRAS*, 337, 109
 Nelson, C. H. 2001, *ApJ*, 544, L91
 Nicastro, F. 2000, *ApJ*, 530, L65
 Onken, C. A., et al. 2004, *ApJ*, 615, 645
 Peterson, B. M. 2004, *ApJ*, 613, 682
 Richards, G. T., et al. 2006, *ApJS*, 166, 470
 Rix, H. W., White, S. D. M. 1992, *MNRAS*, 254, 389
 Sargent, W. L. W., Schechter, P. L., Boksenberg, A., Shortridge, K. 1977, *ApJ*, 212, 326
 Shields, J. C., Rix, H., McIntosh, D. H., Ho, L. C., Rudnick, G., Filippenko, A. V., Sargent, W. L. W., Sarzi, M. 2000, *ApJ*, 534, L27
 Storchi-Bergmann, T., Baldwin, J. A., Wilson, A. S. 1993, *ApJ*, 410, L11
 Strateva, I. V., et al. 2003, *AJ*, 126, 1720
 Strateva, I. V., et al. 2006, *ApJ*, 651, 749
 Tonry, J., & Davis, M. 1979, *ApJ*, 84, 1511
 Tremaine, S., et al. 2002, *ApJ*, 574, 740
 Vanden Berk, D. E., et al. 2006, *AJ*, 131, 84
 Vestergaard, M. 2002, *ApJ*, 571, 733
 Wang, T.-G., Dong, X.-B., Zhang, X.-G., Zhou, H.-Y., Wang, J.-X., Lu, Y.-J. 2005, *ApJ*, 625, L35
 Watson, L. c., Grupe, D., Mathur, S. 2007, *ApJ*, 133, 2435
 Wills, B.J., Browne, I.W.A. 1986, *ApJ*, 302, 56
 Woo, J. H. et al. 2006, *ApJ*, 645, 900
 Wu X.-B., Wang R., Kong M. Z., Liu F. K., Han J. L. 2004, *A&A*, 424, 793
 Wu, X.-B., Liu, F. K. 2004, *ApJ*, 614, 91
 Zhang, X. G., Dultzin-Hacyan D., Wang, T.G. 2007, *MNRAS*, 377, 1215
 Zheng, W., Veilleux, S., Grandi, S. A. 1991, *ApJ*, 381, 418
 Zhou, H. Y. et al. 2006, *ApJS*, 166, 128

TABLE 1
RESULTS FOR 52 DOUBLE-PEAKED AGNS.

| Name (1) | z (2) | EW(Ca K) (3) | χ^2 (4) | FC (5) | S/N (6) | σ_* (7) | σ_*^c (8) | σ_g (9) | $\lambda L_\lambda(5100\text{\AA})$ (10) | M_{bh} (11) | $L_{\text{bol}}/L_{\text{Edd}}$ (12) | ΔV (13) |
|---------------------------|----------|-----------------|-----------------|-----------|------------|-------------------|---------------------|-------------------|---|-------------------------|---|--------------------|
| SDSS J000815.46-104620.57 | 0.199 | -3.5 ± 1.3 | 0.86 | 0.45 | 4.12 | :148.30 | 146.37 | 112.2 ± 4.6 | 43.71 | 7.59 | -1.02 | 3100 |
| SDSS J011140.03-095834.94 | 0.207 | -3.7 ± 0.7 | 0.91 | 0.58 | 3.49 | :110.93 | 110.87 | 92.5 ± 31.1 | 43.77 | 7.10 | -0.48 | 2300 |
| SDSS J013407.88-084129.98 | 0.070 | -7.7 ± 0.6 | 1.07 | 0.07 | 9.47 | 121.14 | 121.14* | 84.8 ± 1.3 | 42.95 | 7.25 | -1.45 | 3800 |
| SDSS J014901.08-080838.23 | 0.210 | -3.1 ± 7.0 | 1.05 | 0.64 | 2.78 | :125.25 | 124.48 | 169.9 ± 5.3 | 43.67 | 7.30 | -0.77 | 2800 |
| SDSS J023253.42-082832.10 | 0.265 | -2.7 ± 0.6 | 0.86 | 0.30 | 11.00 | :186.03 | 182.22 | 236.1 ± 14.3 | 43.97 | 7.97 | -1.14 | 3200 |
| SDSS J024052.82-004110.93 | 0.247 | -3.0 ± 0.3 | 1.31 | 0.67 | 7.52 | 121.61 | 121.02 | 105.9 ± 3.9 | 44.22 | 7.25 | -0.18 | 3100 |
| SDSS J024703.24-071421.59 | 0.333 | -4.3 ± 2.3 | 0.81 | 0.62 | 3.41 | :293.48 | 284.29 | 402.1 ± 19.0 | 44.08 | 8.74 | -1.81 | 8100 |
| SDSS J024840.03-010032.68 | 0.184 | -4.7 ± 1.5 | 0.72 | 0.38 | 6.26 | :155.34 | 153.06 | 91.9 ± 0 | 43.62 | 7.66 | -1.19 | 2700 |
| SDSS J025220.89+004331.32 | 0.170 | -1.3 ± 0.2 | 1.01 | 0.50 | 6.81 | 174.65 | 171.41 | 195.7 ± 6.9 | 43.82 | 7.86 | -1.18 | 2600 |
| SDSS J025951.71-001522.78 | 0.102 | -2.5 ± 0.5 | 0.90 | 0.62 | 4.51 | :137.38 | 136.00 | 116.1 ± 19.3 | 43.28 | 7.46 | -1.33 | 3600 |
| SDSS J034931.03-062621.05 | 0.287 | -5.1 ± 0.8 | 0.98 | 0.61 | 4.32 | :148.31 | 146.38 | 155.0 ± 9.2 | 44.09 | 7.59 | -0.64 | 5300 |
| SDSS J081700.40+343556.34 | 0.062 | -7.6 ± 1.5 | 1.33 | 0.16 | 9.35 | 172.92 | 172.92* | 200.8 ± 4.3 | 43.08 | 7.88 | -1.94 | 6300 |
| SDSS J081916.28+481745.48 | 0.223 | -2.6 ± 0.4 | 1.06 | 0.61 | 4.84 | :173.85 | 170.65 | 170.6 ± 166.4 | 43.97 | 7.85 | -1.03 | 5400 |
| SDSS J082133.60+470237.33 | 0.128 | -7.9 ± 2.9 | 0.90 | 0.19 | 9.47 | 171.11 | 168.05 | 172.8 ± 6.5 | 43.58 | 7.83 | -1.39 | 5200 |
| SDSS J084535.37+001619.52 | 0.260 | -5.2 ± 1.8 | 0.77 | 0.33 | 6.52 | 106.66 | 106.82 | 113.3 ± 9.5 | 43.82 | 7.04 | -0.36 | 5600 |
| SDSS J091459.05+012631.30 | 0.198 | -3.2 ± 0.3 | 0.80 | 0.33 | 11.38 | 156.94 | 154.59 | 180.7 ± 15.5 | 43.97 | 7.68 | -0.86 | 7400 |
| SDSS J092515.00+531711.91 | 0.186 | -3.9 ± 0.7 | 0.79 | 0.26 | 8.78 | 203.50 | 198.82 | 142.7 ± 11.1 | 43.85 | 8.12 | -1.42 | 3400 |
| SDSS J100443.43+480156.45 | 0.199 | -5.6 ± 1.5 | 1.00 | 0.52 | 3.92 | :172.93 | 169.77 | 115.2 ± 3.3 | 43.79 | 7.84 | -1.20 | 6600 |
| SDSS J101405.89+000620.36 | 0.141 | -7.6 ± 1.1 | 1.50 | 0.26 | 12.21 | 221.51 | 215.92 | 166.8 ± 6.5 | 43.85 | 8.26 | -1.56 | 9000 |
| SDSS J103202.41+600834.47 | 0.294 | -2.7 ± 1.0 | 0.82 | 0.55 | 5.30 | 179.60 | 176.11 | 164.1 ± 8.1 | 43.98 | 7.91 | -1.08 | 3700 |
| SDSS J104108.18+562000.32 | 0.230 | -3.5 ± 0.9 | 1.04 | 0.43 | 6.20 | 205.50 | 200.72 | 181.9 ± 0.2 | 43.82 | 8.14 | -1.47 | 8500 |
| SDSS J104128.60+023204.99 | 0.182 | -4.6 ± 0.5 | 0.91 | 0.27 | 9.75 | 185.68 | 181.88 | 191.1 ± 26.2 | 43.78 | 7.96 | -1.33 | 5700 |
| SDSS J104132.78-005057.46 | 0.303 | -3.1 ± 0.3 | 1.41 | 0.47 | 10.42 | 179.70 | 176.20 | 195.1 ± 4.2 | 44.24 | 7.91 | -0.81 | 4500 |
| SDSS J110742.76+042134.18 | 0.327 | -2.5 ± 0.6 | 0.99 | 0.42 | 6.12 | 205.09 | 200.32 | 251.5 ± 13.6 | 44.18 | 8.13 | -1.10 | 3700 |
| SDSS J113021.41+005823.04 | 0.132 | -6.9 ± 1.0 | 0.98 | 0.31 | 10.85 | 148.10 | 146.19 | 95.2 ± 0.9 | 43.73 | 7.58 | -1.00 | 2100 |
| SDSS J113633.08+020747.65 | 0.239 | -4.2 ± 0.3 | 1.18 | 0.74 | 6.41 | 143.45 | 141.76 | 163.2 ± 10.2 | 44.22 | 7.53 | -0.45 | 2500 |
| SDSS J114051.58+054631.13 | 0.132 | -11.2 ± 3.9 | 0.78 | 0.41 | 6.43 | 134.19 | 132.97 | 138.7 ± 8.5 | 43.50 | 7.42 | -1.06 | 9100 |
| SDSS J115047.48-031652.95 | 0.149 | -5.4 ± 1.1 | 0.89 | 0.46 | 5.98 | 137.15 | 135.78 | 91.2 ± 3.7 | 43.69 | 7.45 | -0.91 | 4900 |
| SDSS J122009.55-013201.14 | 0.288 | -5.2 ± 1.2 | 0.96 | 0.49 | 6.70 | 186.09 | 182.28 | 179.4 ± 19.5 | 44.02 | 7.97 | -1.09 | 3100 |
| SDSS J130927.67+032251.76 | 0.267 | -2.6 ± 0.5 | 1.30 | 0.36 | 10.66 | 199.92 | 195.42 | 256.1 ± 0.5 | 43.95 | 8.09 | -1.28 | 3000 |
| SDSS J132442.44+052438.86 | 0.116 | -8.8 ± 10.4 | 1.12 | 0.45 | 3.20 | :145.40 | 143.62 | 231.7 ± 8.9 | 42.98 | 7.55 | -1.72 | 9700 |
| SDSS J132834.14-012917.64 | 0.151 | -4.2 ± 1.0 | 1.41 | 0.60 | 4.70 | :154.22 | 152.00 | 180.6 ± 2.2 | 43.64 | 7.65 | -1.16 | 3600 |
| SDSS J133312.42+013023.73 | 0.217 | -2.8 ± 0.8 | 1.03 | 0.55 | 5.18 | 105.37 | 105.59 | 129.0 ± 2.3 | 43.71 | 7.01 | -0.45 | 3400 |
| SDSS J133338.30+041803.94 | 0.202 | -3.0 ± 0.5 | 0.97 | 0.36 | 7.34 | 206.10 | 201.29 | 185.9 ± 16.7 | 43.82 | 8.14 | -1.47 | 4100 |
| SDSS J134617.54+622045.47 | 0.116 | -3.4 ± 0.3 | 1.37 | 0.64 | 7.94 | 153.91 | 151.71 | 114.1 ± 1.3 | 43.73 | 7.65 | -1.07 | — |
| SDSS J140019.27+631426.93 | 0.331 | -2.3 ± 0.5 | 1.05 | 0.83 | 5.08 | 204.44 | 199.71 | 167.1 ± 25.5 | 44.59 | 8.13 | -0.69 | 5300 |
| SDSS J141454.55+013358.55 | 0.269 | -4.1 ± 0.7 | 1.15 | 0.29 | 10.97 | 218.93 | 213.47 | 287.8 ± 8.6 | 44.03 | 8.24 | -1.36 | 2700 |
| SDSS J141613.37+021907.82 | 0.158 | -5.9 ± 1.2 | 1.02 | 0.54 | 6.70 | 212.96 | 207.80 | 117.6 ± 0.2 | 43.81 | 8.20 | -1.54 | 5900 |
| SDSS J141946.06+650353.04 | 0.148 | -3.7 ± 0.3 | 1.18 | 0.55 | 8.11 | 149.36 | 147.38 | 154.9 ± 6.3 | 43.85 | 7.60 | -0.90 | 2700 |
| SDSS J142754.76+635448.42 | 0.145 | -4.2 ± 0.3 | 1.39 | 0.70 | 7.33 | 159.98 | 157.48 | 117.2 ± 9.5 | 43.86 | 7.71 | -0.99 | 4500 |
| SDSS J143455.31+572345.37 | 0.175 | -2.0 ± 0.4 | 1.65 | 0.51 | 10.09 | 191.25 | 187.18 | 202.6 ± 35.9 | 44.00 | 8.01 | -1.17 | 3100 |
| SDSS J154534.55+573625.12 | 0.268 | -2.2 ± 0.4 | 0.92 | 0.46 | 9.34 | 193.04 | 188.88 | 180.6 ± 4.9 | 44.12 | 8.03 | -1.05 | 2700 |
| SDSS J170102.28+340400.60 | 0.094 | -2.7 ± 0.4 | 1.62 | 0.75 | 3.79 | :127.55 | 126.66 | 118.9 ± 1.4 | 43.28 | 7.33 | -1.20 | 1600 |
| SDSS J172102.47+534447.29 | 0.192 | -5.0 ± 2.4 | 0.78 | 0.35 | 4.45 | :125.66 | 124.86 | 138.7 ± 5.6 | 43.60 | 7.31 | -0.85 | 3400 |
| SDSS J210109.58-054747.31 | 0.179 | -6.2 ± 1.4 | 0.85 | 0.32 | 7.52 | 177.42 | 174.04 | 168.0 ± 15.1 | 43.75 | 7.89 | -1.29 | 3700 |
| SDSS J214935.23+113842.04 | 0.239 | -9.5 ± 5.7 | 0.85 | 0.56 | 1.92 | :178.69 | 175.24 | 132.8 ± 10.0 | 43.66 | 7.90 | -1.38 | 1080 |
| SDSS J222132.41-010928.76 | 0.288 | -6.3 ± 1.1 | 0.84 | 0.56 | 5.01 | 190.63 | 186.59 | 220.5 ± 14.9 | 44.12 | 8.01 | -1.03 | 8200 |
| SDSS J223302.68-084349.13 | 0.058 | -7.2 ± 0.6 | 1.68 | 0.37 | 10.05 | 121.19 | 121.19* | 89.7 ± 0.9 | 43.09 | 7.26 | -1.31 | 2500 |
| SDSS J223336.71-074337.10 | 0.174 | -4.6 ± 0.9 | 0.96 | 0.36 | 9.12 | 145.42 | 143.64 | 192.2 ± 16.4 | 43.58 | 7.55 | -1.12 | 3100 |
| SDSS J230545.67-003608.55 | 0.269 | -7.1 ± 2.3 | 0.93 | 0.35 | 5.52 | 208.17 | 203.25 | 167.4 ± 9.8 | 44.00 | 8.16 | -1.30 | 8200 |
| SDSS J232721.96+152437.31 | 0.046 | -5.2 ± 0.1 | 2.10 | 0.45 | 18.59 | 221.87 | 221.87* | 165.3 ± 0.4 | 43.45 | 8.31 | -2.01 | 4400 |
| SDSS J235128.77+155259.15 | 0.096 | -2.8 ± 0.2 | 1.21 | 0.66 | 6.96 | 155.30 | 153.03 | 112.1 ± 2.9 | 43.66 | 7.66 | -1.15 | 3700 |

NOTE. — Col. (1): Object name. Col. (2): Redshift. Col. (3): Equivalent width of Ca K and the error in units of \AA . Col. (4): χ^2 . Col. (5) fraction of featureless continuum component. Col. (6): effective S/N from the S/N at 4020 \AA and the fraction of featureless continuum component. Col. (7): Uncorrected stellar velocity dispersion in units of km s^{-1} , and values for objects with effective S/N < 5 are preceded by a colon. Col. (8): Corrected stellar velocity dispersion in units of km s^{-1} . For 4 objects with Ca II triplet, it is not need to do the correction which are shown as *. Col. (9): Corrected gas velocity dispersion in units of km s^{-1} . Col. (10): log of the monochromatic luminosity at 5100 \AA in units of ergs s^{-1} . Col. (11): log of SMBH masses from corrected stellar velocity dispersion in units of M_\odot . Col. (12): The Eddington ratios. Col. (13): The peak separations in units of km s^{-1} .